https://doi.org/10.48047/AFJBS.6.15.2024.1469-1490

African Journal of Biological Sciences

Research Paper Open Access

DEVELOPING TRIAZOLOPIPERAZINE DERIVATIVES AS DPP-4 INHIBITORS: A COMPUTATIONAL STUDY FOR IMPROVED SAFETY PROFILE IN TYPE 2 DIABETES MELLITUS MANAGEMENT

Shahin Muhammed TK[1,3]*, Sarath Chandran C [1,3], Balakrishnan Valliyot[2,3], Ammu KM[1], Archana O[1], Adithya KP[1], Achyut Aravind[1]

[1]College of Pharmaceutical Sciences, Government Medical College, Pariyaram-670503, Kannur, Kerala, India

[2]Department of Medicine, Government Medical College, Pariyaram-670503, Kannur, Kerala, India

[3]Kannur University, Kannur-670002, Kerala, India

Email ID: **shahin.mdtk@gmail.com**

Article History

Volume 6, Issue 15, 2024

Received : 11 Jun 2024

Accepted : 07 Sep 2024

doi: 10.48047/AFJBS.6.15.2024.1469-1490

Abstract

Type 2 Diabetes Mellitus (T2DM), a prevalent metabolic disorder characterized by insulin resistance and impaired secretion, is treated with five FDA-approved medications, namely sulfonylureas, meglitinides, biguanides, thiazolidinediones, α-glucosidase inhibitors, and dipeptidyl peptidase-4 (DPP-4) inhibitors. However, these drugs have adverse effects, prompting researchers to investigate DPP-4 inhibitors (gliptins) for their improved safety profiles. In this study, triazolopiperazine derivatives were developed as DPP-4 inhibitors using the Schrödinger Suite 2022-1, integrating field-based Quantitative Structure Activity Relationship (QSAR), molecular docking, and molecular dynamics (MD) simulations. Forty-five triazolopiperazine derivatives with IC50 values from 0.43 nM to 455 nM were used to develop spatial characteristics via Gaussian field-based QSAR, yielding promising statistical results. Contour maps revealed favorable and unfavorable interactions around the triazolopiperazine nucleus, leading to the design of 10 new compounds with improved predicted IC50 values, strong binding affinities, and docking scores. Compound G86 demonstrated superior binding affinity and inhibitory activity against DPP-4 compared with sitagliptin, suggesting its potential for further development. QikProp analysis predicted favorable pharmacokinetic and physicochemical properties and a better safety profile for G86, whereas MD simulations showed that the G86-1X70 complex was more stable than the sitagliptin-1X70 complex. This study highlights the effectiveness of computational methods in accelerating anti-diabetic drug discovery and facilitates future research and therapeutic advancements in T2DM management.

Keywords: DPP-4 Inhibitors, Type 2 Diabetes Mellitus, Docking, Field-based QSAR, Molecular Dynamics, Triazolopiperazine.

1. Introduction

Diabetes Mellitus (DM) is a group of metabolic disorders characterized by abnormal plasma glucose levels. There are two primary types of DM: Type 1 Diabetes Mellitus (T1DM), also known as insulin-dependent Diabetes Mellitus and T2DM, also known as non-insulin-dependent diabetes mellitus (NIDDM)(1,2). T2DM, or NIDDM, is the most prevalent form, and is characterized by impaired insulin sensitivity or insulin resistance, decreased insulin production, and hyperglycemia(3,4). It is anticipated that the number of people with diabetes will increase dramatically to 643 million worldwide by 2030. Moreover, estimates suggest that by 2045, this figure will rise even further, impacting almost 783 million individuals globally(5). Individuals diagnosed with T2DM are at a heightened risk for both macrovascular and microvascular complications, including peripheral vascular and renal disorders, hypertension, cardiovascular diseases, neurological conditions, and retinopathy. The U.S. The Food and Drug Administration has approved five main groups of medications to address glucose imbalance and reduce the risk associated with type 2 diabetes: sulfonylureas, non-SU secretagogues (meglitinides), thiazolidinediones, biguanides, α-glucosidase inhibitors, and recently approved dipeptidyl peptidase-4 (DPP-4) inhibitors(6). Traditional medications often show diminished efficacy over time, leading to inadequate glycemic control. Furthermore, a few of these medications have side effects such as weight gain, hypoglycemia, and gastrointestinal irritation. Therefore, there is a need for alternative therapies that can address the limitations of conventional antihyperglycemic medications (7). Maintaining the balance of glucose requires the action of hormones, such as glucose-dependent insulinotropic polypeptide (GIP) and glucagon-like peptide (GLP-1). This is achieved by promoting insulin synthesis and release by supporting pancreatic β-cell activity. GLP-1 enhances glycemic control by reducing appetite and increasing the responsiveness of β-cells to glucose. GLP-1 and GIP enzymes are broken down by DPP-4, which is a multifunctional membrane-anchored serine ectopeptidase. By inhibiting DPP-4, their breakdown can be prevented, leading to increased insulin release in response to glucose. It should be noted that current anti-diabetic drugs are becoming less effective owing to adverse effects such as hypoglycemia, obesity, nausea, and gastric problems. As a result, researchers are working

to develop powerful drugs with fewer adverse effects, such as DPP-4 inhibitors or gliptins, which offer long-term glycemic control and reduce the risk of hypoglycemia. The most popular drugs for inhibiting DPP-4 are sitagliptin and vildagliptin, which are competitive and reversible. They exhibit delayed binding inhibition kinetics and are rapidly absorbed orally. The core nuclei of DPP-4 inhibitors mainly include cyanopyrrolidines, triazolopiperazine amides, and pyrrolidines. Piperazine analogs have potent anti-diabetic properties, so they are frequently utilized as DPP-4 inhibitors. In this study, the DPP-4 inhibitory action of triazolopiperazine derivatives was investigated(1). A variety of triazolopiperazines with improved IC50 values have been described by replacing the nitrogen atom from positions 2 to 3 in sitagliptin molecules (Figure 1) (7).

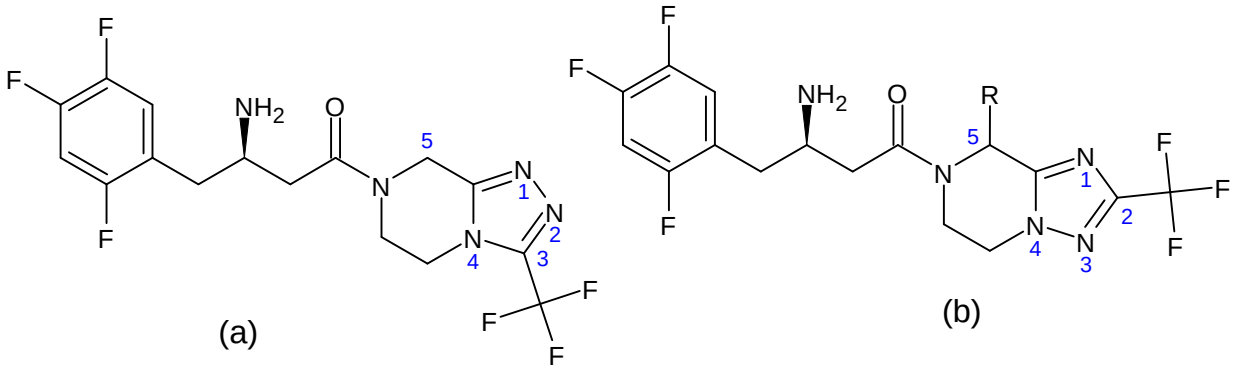

Figure 1: Chemical structure of (a) sitagliptin and (b) its derivative (8)

2. Materials and methods

2.1 Details about computers and software

The study endeavors included docking, MD simulation, field-based QSAR, preparation of both the ligand and the protein, and ADME computation using Schrödinger (v. 2022-1) software(9,10).

2.2 Field based 3D QSAR modelling

Using a field-based technique, a library of 45 ligands was constructed to build 3D-QSAR models, which are three-dimensional quantitative structure-activity relationships. (11). Predictions were generated by randomly dividing the ligands into the training (70%) and testing (30%) sets. Partial least squares (PLS) factors were used to linearly fit the five Gaussian parameters (hydrogen bond acceptor, hydrogen bond donor, hydrophobic, steric, and electrostatic). These five indicators were used for the highest total of PLS factors in the linear regression statistics. The study of values for Pearson's r, root mean squared

error (RMSE), cross-regression coefficient (Q2), standard deviation (SD), and regression coefficient (R2) led to the selection of the best QSAR model. The optimal model was analyzed using five different colored contour maps to show the intended spatial configurations of the functional moieties (10, 13, 14). Approximately 100 molecules (G1-G100) were designed based on the QSAR model by replacing the appropriate groups on the positive counters and avoiding groups that would lead to negative effects. Ten compounds were selected that yielded better predicted IC50 values.

2.3 Ligand preparation

A collection of 45 congeneric triazolopiperazine derivatives (A1-A45) with DPP-4 inhibitory activity and IC50 values ranging from 0.43 to 455 nM were compiled from journals and BindingDB. Ten compounds were predicted using QSAR, resulting in a total of 55 compounds being selected for further analysis. The ligand was prepared using the LigPrep feature of Maestro's Epik tool, and the OPLS4 force field was used to generate the lowest energy conformer per ligand. The pH was then neutralized. LigPrep is an advanced tool designed to generate high-resolution three-dimensional structures with all atoms for a variety of compounds with drug-like properties. Beginning with either 2D or 3D structures, it may produce structures in the SD or Maestro format. For each correctly processed input structure, LigPrep generated an exclusive low-energy three-dimensional representation with exact chiralities. It may also consider various ring conformations, stereochemistry, tautomers, and ionization states to produce numerous structures from each input. Additionally, it allows for the removal of molecules based on parameters such as molecular weight or specific functional groups.(9,12)

2.4 Protein preparation

In scientific research, the process of preparing polypeptides for molecular docking is referred to as the polypeptide setup. This procedure involves several processes such as optimization, hydrogen bond addition, atomic collision removal, and water molecule deletion from the crystal structure of the protein. The Protein Data Bank (<https://www.rcsb.org/>) provides the 3D crystal structure of the human DPP-4 protein (1X70)(13,14) in association with triazolopiperazine (the comparative medication, sitagliptin). The results for the protein structure 1X70 were good, showing an observed R-value of 0.193, a free R-

value of 0.228, and a resolution of 2.10 Å. Using Maestro's Protein Preparation Wizard (Schrödinger, LLC, New York, NY, USA), the protein was constructed by removing water molecules, adding lacking hydrogen atoms, and modifying the bond ordering and charges. The ProtAssign algorithm was employed to maximize the hydrogen-bonding (H-bond) network by investigating the neutral and protonated states and flipping terminal chi angles for specific amino acids. The H-bond network can operate in either a "standard" mode, which takes seconds to complete, or an "exhaustive" mode, which takes minutes to hours depending on the complexity of the network. During protein preparation, the entire structure was relaxed using the force field OPLS4 and the Impref tool was used for H-bond optimization(9,15).

2.5 Receptor grid generation

Schrödinger's Maestro receptor grid-generating module was used to create a grid around a protein binding site. To appropriately score the ligand postures, a grid is necessary. Upon contact, receptors may undergo conformational alterations, including modifications of side chain or loop conformations. The chosen region is recognized as the receptor that determines its structure and characteristics. Atoms from sites where ligands were present were selected using the input mode. The van der Waals radius of the atoms of the receptor was manipulated, and an enclosed box created a grid centered on the designated residue within a ligand length of ≤20 Å(16,17).

2.6 Molecular docking

Molecular docking, a widely employed technique in molecular modelling, is used to investigate the interactions between ligands and receptors and determine how best to align a ligand with a target receptor(18). Researchers have employed a thorough examination of the ligand torsion-angle region within the ligand-receptor interaction environment to select ligand conformations, which are subsequently represented in a concise combinatorial form. Initial screens involve exploration of the entire phase space of the ligand. Notably, the Glide approach employs truncations and approximations to enhance the computational efficiency while maintaining systematic search methods. Then, using the OPLS-4 force field and a distance-dependent dielectric approach, the ligand was minimized inside the receptor field. The three to six lowest-energy positions underwent a Monte Carlo process to identify the

local torsional minima. The GlideScore scoring function, which is a refined ChemScore algorithm, ranks ligands for screening and predicts binding affinity. When choosing the proper docked pose, Emodel, an integrated ranking algorithm that combines GlideScore, ligand-receptor molecular mechanics contact energy, and ligand strain energy, performs better than GlideScore and molecular mechanics energy alone(19). The GLIDE tool was used to evaluate the ligand versatility and protein-ligand binding power (kcal/mol) in a molecular docking investigation of 55 compounds using Maestro software(9). Glide XP docking calculations used a prepared protein grid file, and the XP Glide scoring function ranked the top compounds. The XP visualizer analyzed specific interactions such as π-cation and π-π stacking(16). Hit molecules have been identified through the examination of hydrophobic, π-π stacking, and H-bonding interactions(9). The performance of the technique was evaluated in molecular docking studies involving ten ligands with superior predicted IC50 values compared to the forty-five triazolopiperazine derivatives.

2.7 ADME and toxicity prediction

In the realm of drug research and discovery, predicting bioavailability is a critical aspect, as it often leads to the failure of potential drugs in the early stages of clinical trials owing to inadequate pharmacokinetic properties. The Absorption, Distribution, Metabolism, and Excretion (ADME) characteristics of eight compounds with high docking scores were assessed using the Maestro program, especially the QikProp tool. Pharmacokinetic features such as aqueous solubility, hydrophobicity, oral absorption by humans, permeability of the blood-brain barrier, and gastrointestinal permeability are all determined by these characteristics(9). Prior to using QikProp in the normal mode, each molecule must be neutralized because the tool does not neutralize molecules and produces descriptors in this manner. Approximately 44 features were predicted by QikProp, comprising fundamental descriptors and physiochemical variables necessary for logical drug design, including the log P value (octanol/water), QP%, log HERG, permeability of Caco-2 cell membranes, permeability of MDCK cells, and Lipinski's rule of five(20). ProTox 3.0 was also used to predict the toxicity class as well as LD50. Toxicity studies were primarily conducted on the ligands with the best predicted IC50 and docking scores.

2.8 Molecular dynamic simulation

Through the application of virtual screening assessments, we had the opportunity explored the stability of the conformations and the temporal binding potential of the ligands inside the DPP-4 binding pocket. The approximate spatial orientation of the ligand was determined using virtual screening. However, a thorough assessment of its binding power and conformational durability is necessary to determine the inhibitory potency of ligands that target DPP-4. To comprehensively scrutinize the conformational landscape of protein-ligand assemblies under physiological circumstances, we utilized MD simulations. Each ligand was subjected to separate MD simulations with the designated target protein using Schrödinger (v. 2022-1) Desmond module. The ensuing MD trajectory served as a tool for examining dynamic balance over a period. By considering the mean simulated configuration of all MD trajectory frames and the root mean square deviation (RMSD) measure of the initial structure, we acquired insights into the convergence of the simulated protein-ligand assemblies. The docked ligands that scored the highest were subjected to MD simulations in 100 ns time segments.

The Protein Preparation Wizard, a part of the Schrödinger suite, was used for the preparation of ligand-receptor assemblies. Wizard carried out various operations, such as recasting of hydrogens and bonds, supplementing missing atoms in the side chain, and optimizing loop amino acid sequences using standard configurations. The System Builder component of Wizard was used to establish a periodic simulation box, which was solvated at pH 7.4, using the TIP3P water model. Opposition ions are introduced to neutralize the environment. The OPLS all-atom force field was applied, along with 1000 iterations of the most severe fall approach, to reduce the energy to its minimum. The primary stage of equilibrium was achieved by simulation of the NPT ensemble (with constant atoms, pressure, and temperature) for a duration of 100 ns, conducted in an unregulated production simulation. The system was monitored using a Nosé–Hoover thermostat (300 K, relaxation time = 1 ps) and an isotropic Martyna-Tobias-Klein barostat (1.01325 bar, relaxation time = 2 ps). The smooth particle mesh Ewald (PME) method was employed to examine long-range Coulomb interactions and short-range interactions (cutoff = 9 Å) using the RESPA integrator. Frames that recorded dynamic movements were extracted at

10 ps intervals. The system's stability was assessed using metrics such as the radius of gyration (Rg), hydrogen bond analysis, torsional bonds, RMSF, and RMSD histograms.(21)

The Desmond program was used to perform computational MD studies to verify and assess the accuracy of the molecular docking. The system used the best force field for liquid simulations, OPLS4, to explore the interactions between the protein under study (PDB ID:1X70) and the G86 molecule, which is well known for its stability at the active site of the receptor. A straightforward point-charged (TIP3P) water model was used for this purpose. The protein atoms and box sides were separated by a 10 Å buffer zone composed of an orthorhombic water box. To ensure neutrality, Na+ ions were added to the system after the removal of any overlapping water molecules. A force field with OPLS4 was used to calculate the energy. A pressure of one atmosphere and a temperature of 300 K were consistently maintained (18). A 100ns duration was utilized for the simulation. Ten picoseconds were The recording interval, yielding approximately ten thousand frames. The radius of gyration (rGy), RMSF, and RMSD are among the metrics used to evaluate MD trajectory(9). MD simulations were performed for the reference sitagliptin (A44), the best-selected ligand (G86), and the ligand with the highest experimental IC50 reported in the literature (A45).

3. Results and discussion

3.1. Field based QSAR

The 3D QSAR method, based on Gaussian fields, facilitated the forecasting of DPP-4 inhibitory activity and identification of three key spatial attributes for 45 properly aligned triazolopiperazine derivatives (A1-A45). The test and training set statistics included a standard deviation of 0.2005, R^2 value of 0.9166, R^2 with cross-validation of 0.7939, R^2 scramble value of 0.4391, stability of 0.922, F value of 102.6, P value of 3.27e-15, RMSE of 0.37, Q^2 of 0.5912, and Pearson's r of 0.7919 (Table 1). The PLS factor was determined as 3. The model's near-zero SD and RMSE results demonstrated a low error probability at PLS 3. While the Q^2 value in the test set indicated a strong connection, the high R^2 value in the training set indicated a significant relationship between anticipated and actual actions. The significant variance

ratio (F) and minimal error probability (P) of the chosen model demonstrated good predictability. The external validation of the best model was validated by the Pearson r value, which showed a significant relationship between the observed and expected activities in the test set.

PLS Factor	**SD**	**R^2**	**R^2CV**	**R^2 Scramble**	**stability**	**F**	**P**	**RMSE**	**Q^2**	**Pearson-r**
1	0.4110	0.6246	0.4961	0.1445	0.975	49.9	7.455e-08	0.54	0.1523	0.4127
2	0.2982	0.8090	0.6902	0.2508	0.97	61.4	3.76e-11	0.45	0.4088	0.7670
3	0.2005	0.9166	0.7939	0.4391	0.922	102.6	3.27e-15	037	0.5912	0.7919

Table 1 : Field-based parameters for 3D-QSAR modeling

Based on the information gathered from the contour maps, many substituent groups were changed, including the hydrophobic, steric, electrostatic, H-bond donor, and H-bond acceptor groups (Figures 2 and 3). For steric contour illustrations, the yellow contour shows locations that are less conducive to activity for bulky groupings, whereas the green contour shows the reverse. In the context of electrostatic fields, the red contours indicate increased activity from electron-withdrawing groups and the areas with increased activity from electron-donating groups. The favorable position for the hydrogen bond donors is denoted by the blue-violet color, whereas the cyan color signifies a negative interaction. In the case of hydrogen bond acceptors and hydrophobic contours, increased activity is denoted by red and yellow colors, and negative interactions are indicated by magenta and white colors, respectively. Table 2 lists the expected effects of these compounds.

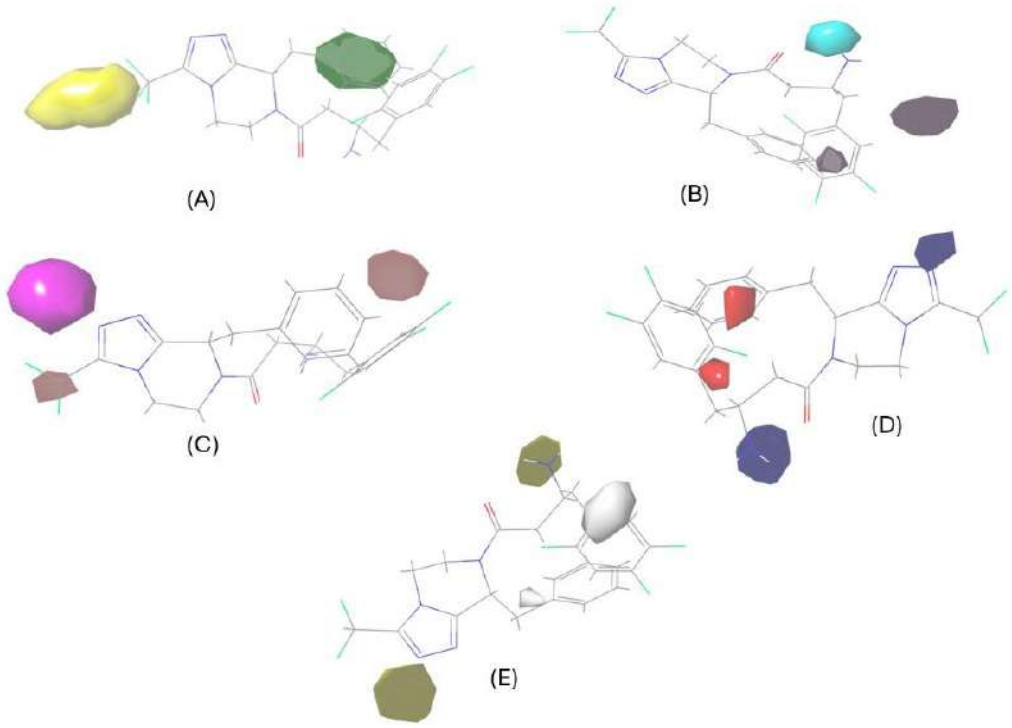

Figure 2: Contour Maps of compound A39 A) Steric B) H-bond donor C) H-bond acceptor D) Electrostatic E) Hydrophobic

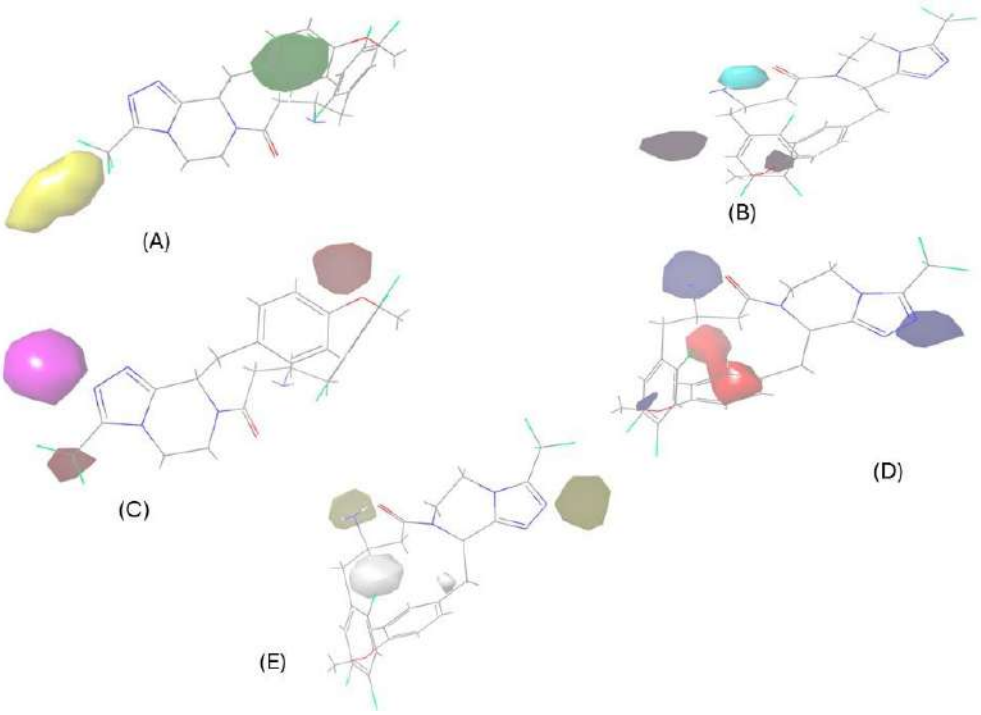

Figure 3 : Contour Maps of compound A45 A) Steric B) H-bond donor C) H-bond acceptor D) Electrostatic E) Hydrophobic

Sl No	Title	Experimental pIC50/ Predicted pIC50
1	A44	7.744727
2	A45	9.366532
3	G1	7.92359
4	G9	8.073709
5	G21	7.939924
6	G55	7.831294
7	G80	7.916484
8	G81	7.920243
9	G82	8.025752
10	G83	8.044069
11	G84	8.045406
12	G86	7.923713

Table 2: Experimental pIC50/Predicted pIC50 of various ligands

3.2 Molecular Docking

In the field of virtual screening, drug design, and lead optimization, molecular docking is a valuable computational approach for identifying new bioactive compounds by analyzing protein-ligand binding interactions. Using Glide Dock XP, triazolopiperazine derivatives were ranked and sorted based on docking scores that were higher than or equal to sitagliptin (9). A total of 55 molecules, including the reference molecule sitagliptin and 10 newly designed molecules, were subjected to molecular docking studies with the 1X70 receptor. The docking scores of compounds G86, G9, and A44 revealed that compound G86 exhibited a strong binding affinity (-10.9 kcal/mol) for the 1X70 receptor, forming

hydrogen bonds with TYR 662, GLU 205, GLU 206, VAL 207, ARG 358, and engaging in pi-pi contacts with PHE 357 as well as TYR 666 (Figure 4). Compound G9, which was moderately active (-9.5 kcal/mol), had a lower docking score than compound G86 and formed hydrogen bonds with ARG 125, GLU 205, and TYR 662, and pi-pi contacts with PHE 357 and TYR 666 (Figure 5). Compound A44 (sitagliptin), the least active (-9.3 kcal/mol) of the three, formed hydrogen bonds with TYR 662 and GLU 205 and engaged in pi-pi interactions with TYR 666 and PHE 357 (Figure 6). Figures 4-6 show the specific 2D and 3D interactions with the binding of G86, G9, and A44 with the DPP-4 receptor crystal structure. Figure 7 shows the structures and docking scores of the developed compounds.

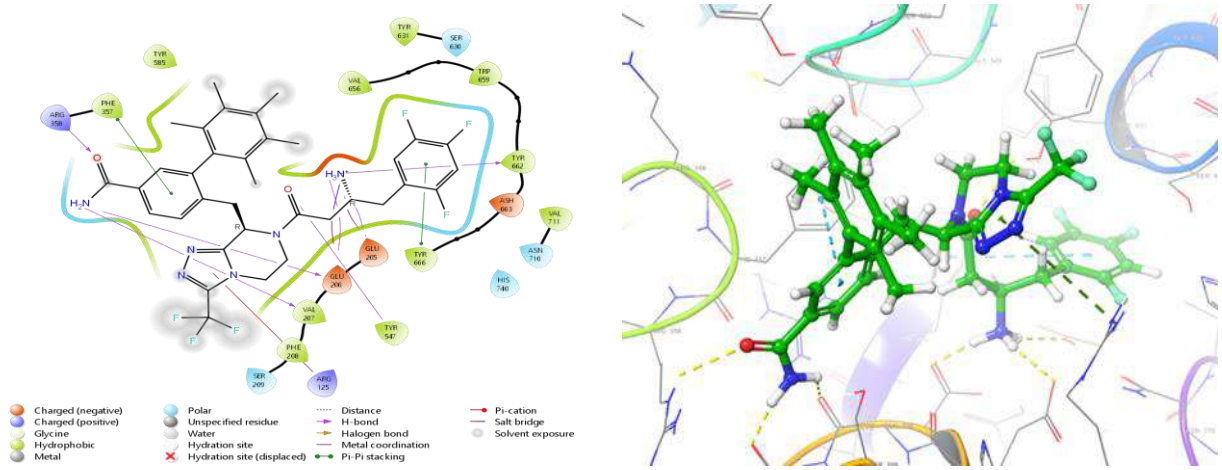

Figure 4:2D & 3D interaction image of ligand G86 with DPP-4 receptor protein (PDBID:1X70)

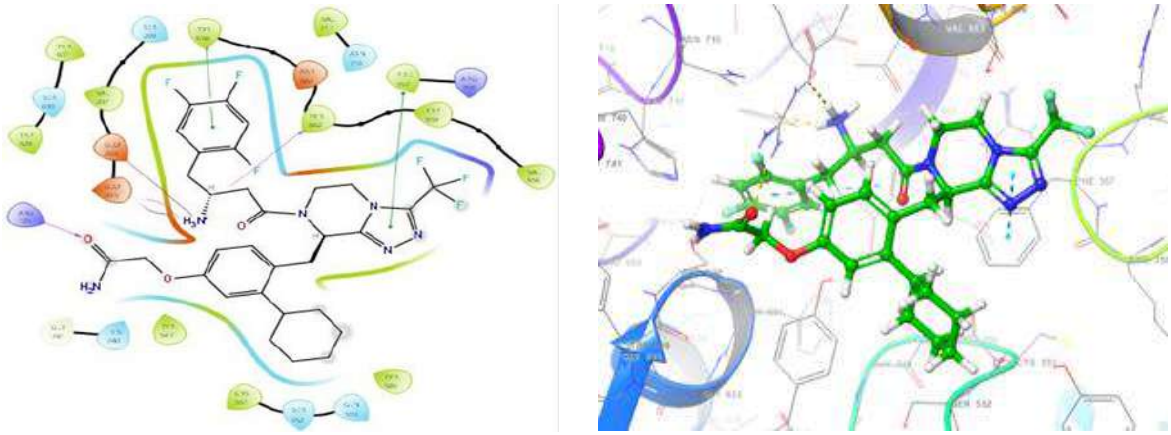

Figure 5:2D & 3D interaction image of ligand G9 with DPP-4 receptor protein (PDB ID:1X70)

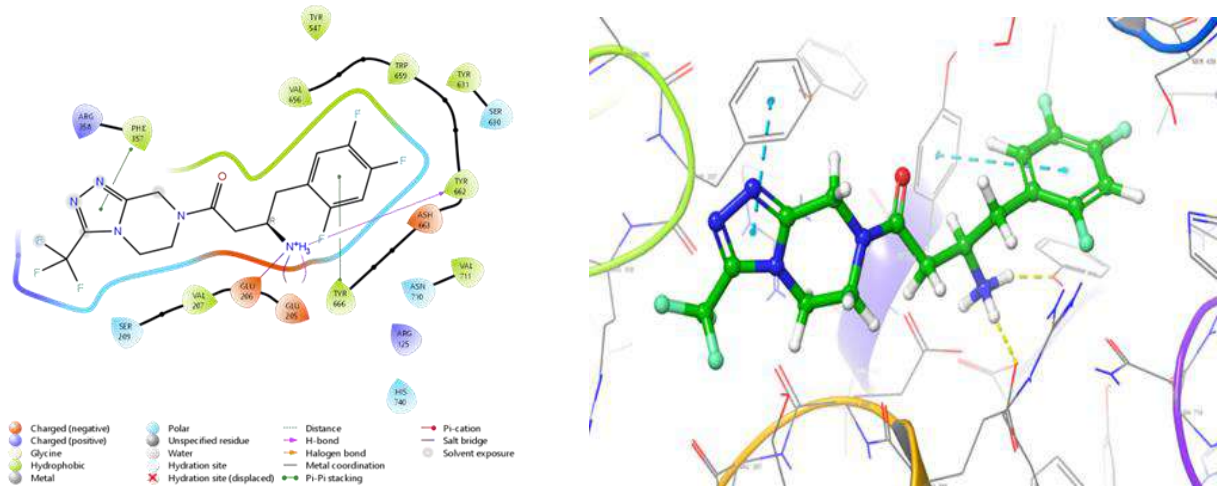

Figure 6:2D & 3D interaction image of ligand A44 (reference) with DPP-4 receptor protein (PDB ID:1X70)

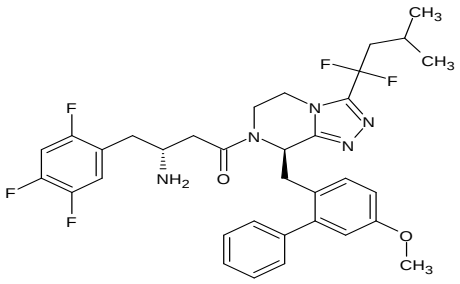

G1 (Dock score: -7.9 Kcal/Mol)

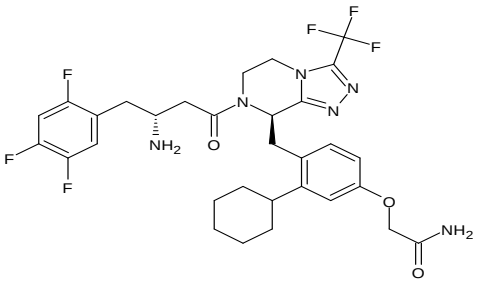

G9 (Dock score: -9.5 Kcal/Mol)

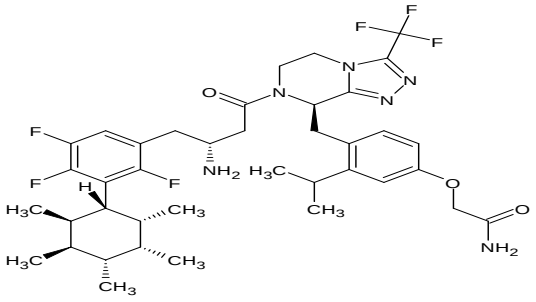

G21 (Dock score: -5.1 Kcal/Mol)

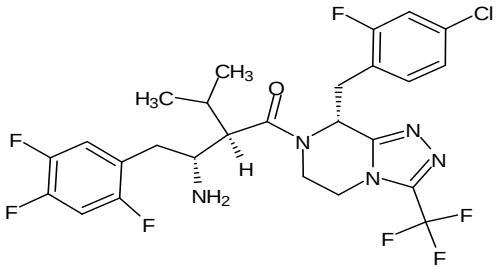

G55 (Dock score: -8.7 Kcal/Mol)

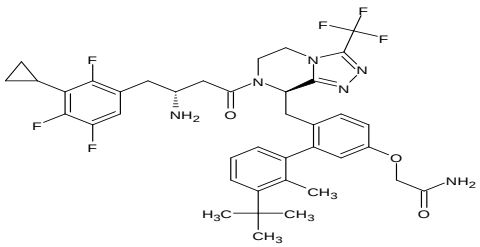

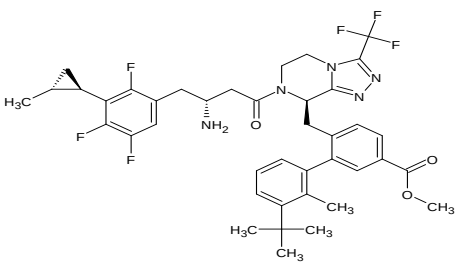

G80 (Dock score: -9.3 Kcal/Mol)

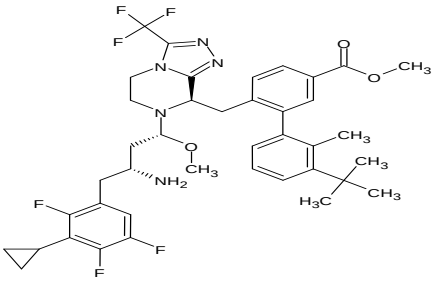

G81 (Dock score: -5.6 Kcal/Mol)

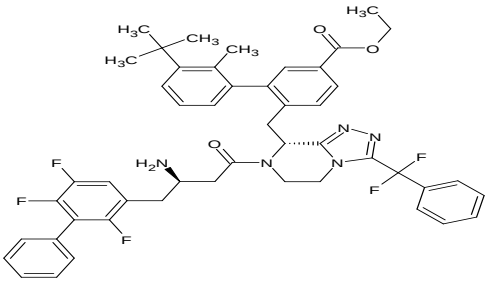

G82 (Dock score: -9.7 Kcal/Mol)

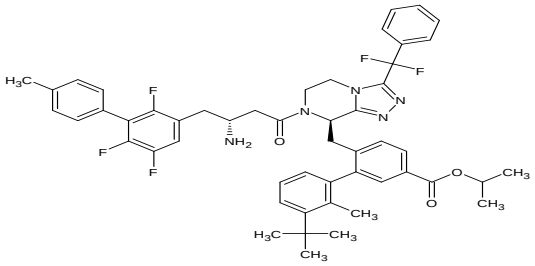

G83 (Dock score: -6.8 Kcal/Mol)

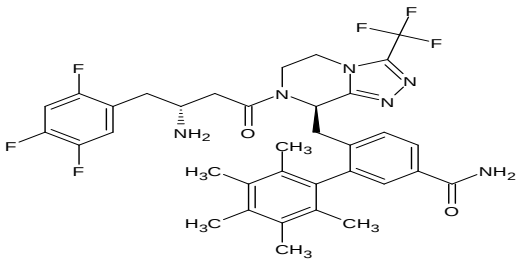

G84 (Dock score: -7.3 Kcal/Mol)

G86 (Dock score: -10.9 Kcal/Mol)

Figure 7 : Structures of designed lead compounds

3.3 ADME calculation

Using Schrödinger's QikProp module, which offers a comprehensive range for comparing the characteristics of a particular molecule to nearly 95% of known medications, the ADMET properties of the eight molecules were evaluated to determine their pharmacokinetic characteristics (Table 3). The coefficients were investigated according to "Lipinski's rule of five." Each compound exhibited a favorable toxicological profile and drug-like ADMET properties. Their molecular weights ranged between 407.318 and 686.699 Da, which fell within the accepted limit of 130–725 Da. The number of hydrogen bond acceptors (HBA) ranged from 5 to 8.7 (Range: 220). The majority of the properties, such as #stars (0-5), #amine (0-1), amidine (0), amide (0-1), donorHB (0-6), QlogPoct (8-35), and QlogPo/w (-2 to 6.5), were within acceptance limits(9). Comprehensive analysis of all pharmacokinetic parameters, such as H-bond acceptor and donor, polar surface area, aqueous solubility, lipophilicity, and permeation across the blood-brain barrier (BBB), identified compound G86 as a promising candidate and was

considered for an MD simulation study. This study involved the analysis of protein-ligand complex stability using reference compounds A44 and A45. The toxicity prediction and predicted LD50 values indicated that the designed compounds exhibited a superior safety profile (Figure 8).

molecule	#stars	#amine	#amidine	#amide	mol_MW	donorHB	acceptHB	QPlogPoct	QPlogPo/w	PercentHumanO
A44	1	1	0	1	407.318	1	5	17.672	3.067	80.67
A39	1	1	0	1	497.442	1	5	20.833	4.911	94.892
A45	2	1	0	1	527.468	1	5.75	21.988	5.251	72.414
G9	4	1	0	2	652.638	3	8.25	32.107	4.834	58.041
G55	2	1	0	1	591.958	1	5	23.277	6.401	81.843
G80	6	1	0	2	756.79	3	8.25	33.743	5.906	59.641
G82	10	2	0	0	757.818	2	8.7	33.106	7.871	79.267
G86	1	1	0	1	686.699	3	7.5	30.709	5.253	57.657

Table 3: ADME profile of the designed compound and the reference compound.

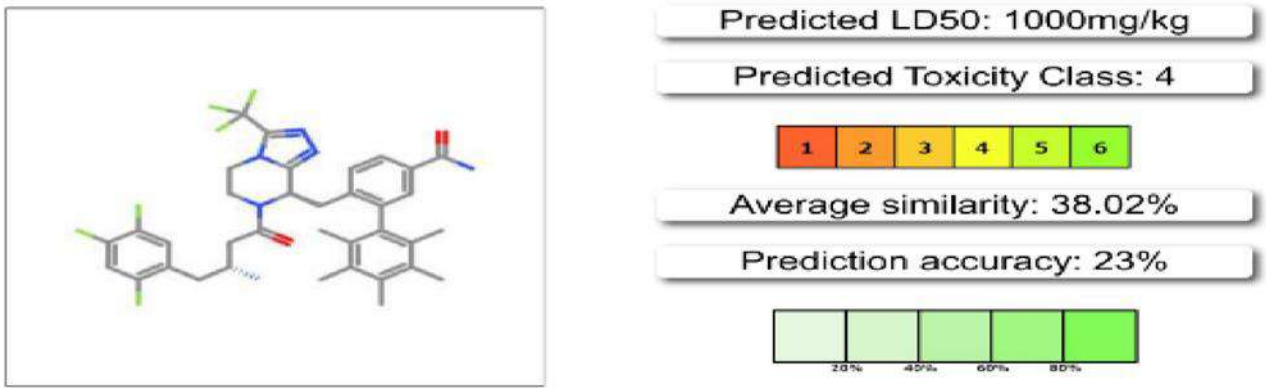

Figure 8: Prediction of G86 toxicity.

3.4 Molecular dynamics

To acquire a deeper understanding of the chemical stability and dynamic characteristics of ligand-protein assemblies, we conducted simulations using MD in an explicit solvent context. These simulations shed light on how ligand attachment influences the structure of proteins and offer a thorough understanding of how protein-ligand interactions contribute to maintaining stable conformations during movement. This is a complete original rephrasing of the content provided. Three protein-ligand complexes were

utilized for the simulations, including one predicted ligand with the highest docking score (G86), one reference compound (A44), and one compound with the highest activity among the congeneric series (A45). The long-term stability and binding affinity of the ligand-protein combination under computer-generated physiological conditions were assessed using MD simulations. A pressure of 1 bar was applied in every simulation run conducted at 300 K. with a relaxation duration of 10 ps. For every simulation, the force field variables from the OPLS4 were used. The MD research results showed that, in contrast to the reference (A44) and the molecule with the greatest activity in the congeneric series (A45), the developed compound (G86) displayed stable interactions.

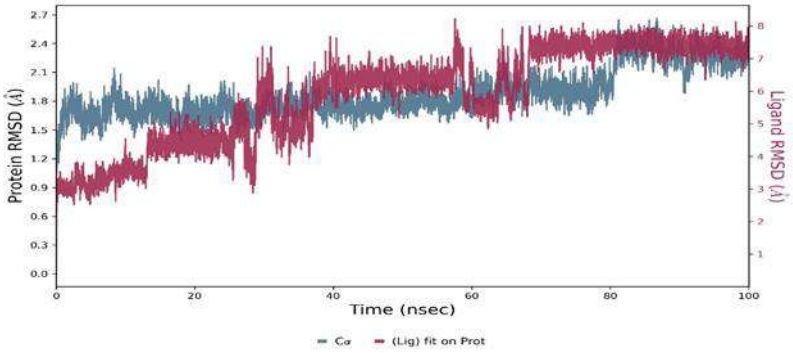

Figure 9 : Protein –Ligand RMSD of G86-1X70 complex

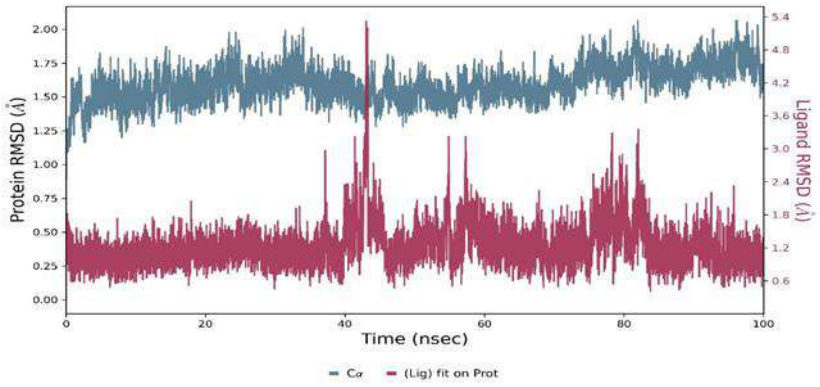

Figure 10: Protein- Ligand RMSD of A44 (Reference)-1X70 complex

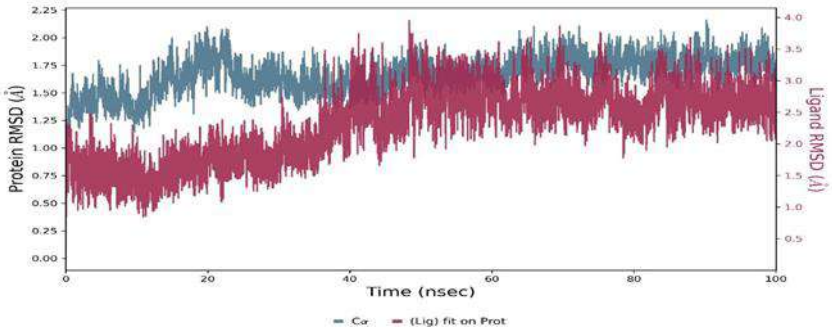

Figure 11: Protein – Ligand RMSD of A45-1X70 complex

The RMSD figure evaluates the difference between the starting locations of the ligand and protein atoms in the binding cavity (0 ns) and at the last moment of the simulation session (100 ns). The degree of stability of the ligand-protein assemblies was measured using this figure. The stability of each system throughout the simulation was evaluated by plotting the RMSD values of the protein backbone atoms over time. In particular, we computed the RMSD measurements versus the simulation duration (0-100 ns) for the 1X70 framework with the ligand G86. The results are shown in Figure 9. Furthermore, we calculated RMSD measurements for the 1X70 backbone in conjunction with A44 (sitagliptin) and A45, benchmarked against a simulation scale ranging from 0 to 100 ns. The results of these calculations are shown in Figures 10 and 11, respectively. It is important to mention that all three paths displayed RMSD values between 1-3 Å throughout the 100 ns simulation, with G86 demonstrating superior stability compared to the benchmark compounds. Variations within the 1-3 Å range were deemed tolerable for small globular proteins. RMSF can be used to examine local alterations along the protein chain. The most variable regions of the protein were indicated by peaks in the RMSF graph. RMSF analysis of the protein with ligand G86 revealed less fluctuation compared to the other two proteins due to increased interactions in the G86-Protein complex (Figure 12).

Protein RMSF

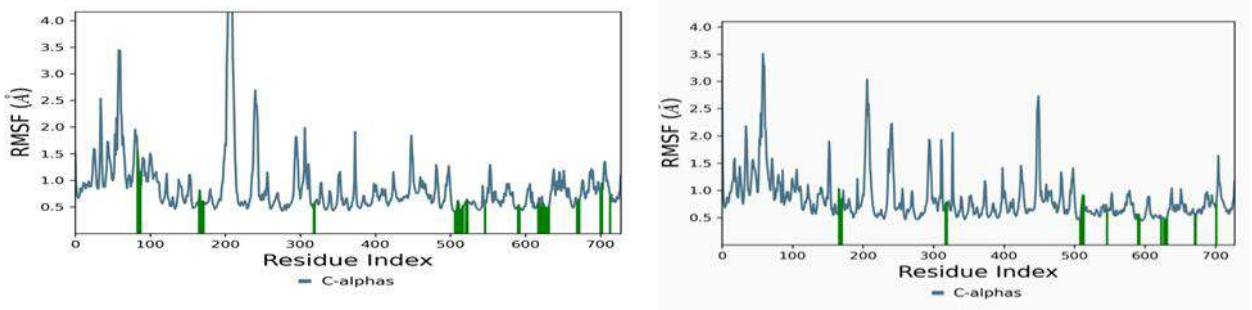

A B

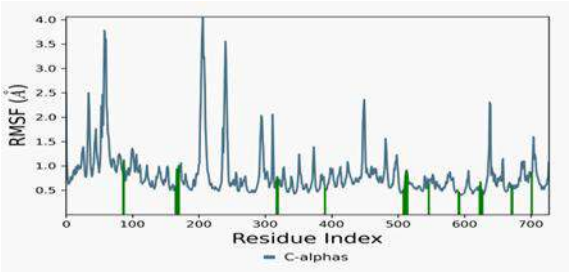

C

Figure 12: Protein RMSF of A) G86 B) A44-Reference C) A45

Ligand RMSF

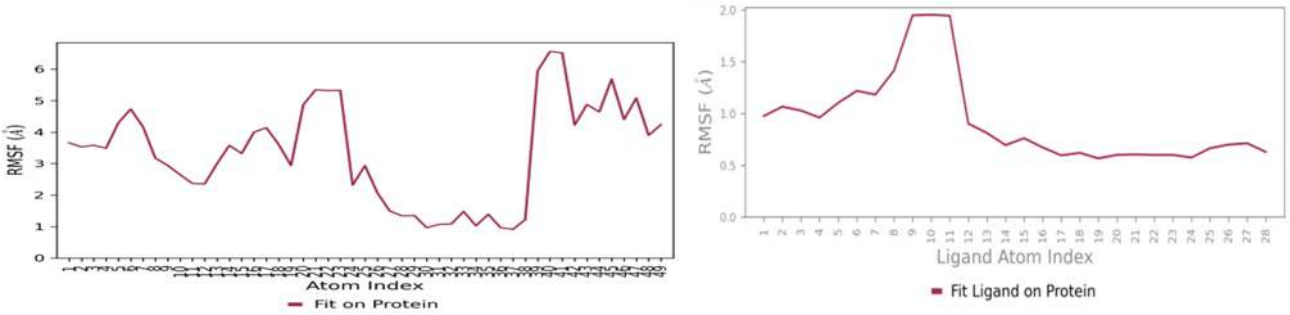

A B

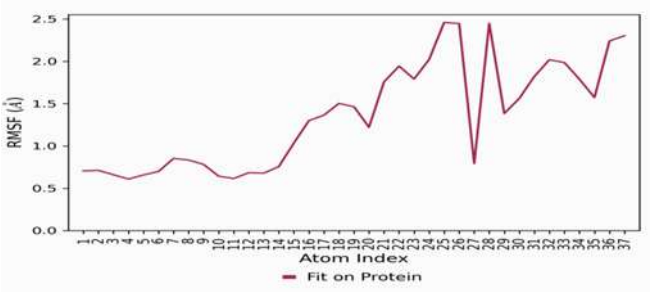

C

Figure 13 : Ligand RMSF of A) G86 B) A44-Reference C) A45

The ligand RMSF serves as a useful instrument for scrutinizing changes in the positions of the ligand atoms. The peaks in the graph indicate significant deviations of the ligand from the reference positions. The L-RMSF for G86 was found to be on par with that of the benchmark medication A44, Sitagliptin, as depicted in Figure 13.

Protein-ligand contact

The protein-ligand contacts provide information about the ligand-protein interactions that occur along the trajectory. Various interactions are possible between the ligand and protein, including water bridges, ionic bonds, hydrophobic interactions, and hydrogen bonds. More specialized subtypes exist within each interaction type. Figure 14 depicts the ligand-protein interactions. These results clearly indicate that the G86-1X70 complex has more contacts than the reference, suggesting its stability.

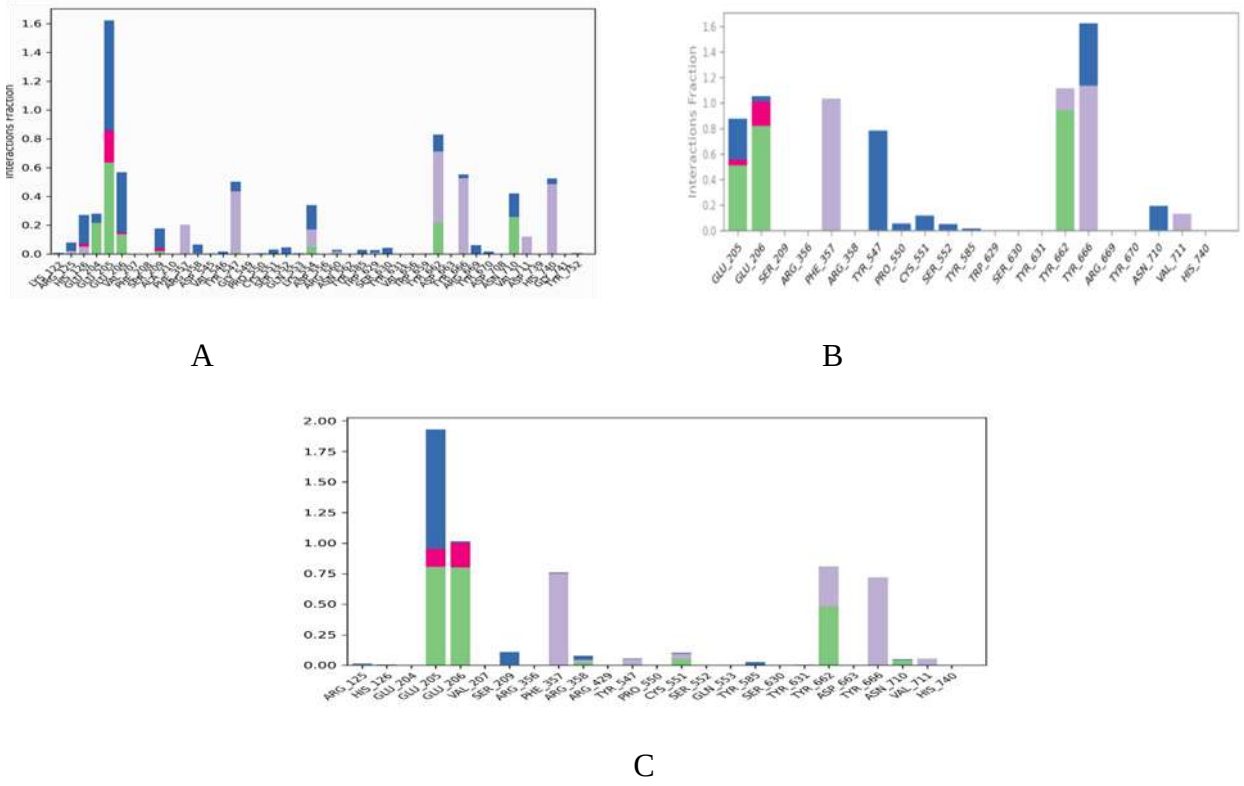

A B

C

Figure 14: Protein ligand contact histogram of A) G86 , B) A44 , C)A45

4. Conclusion

This study aimed to evaluate novel gliptin derivatives as potential treatments for diabetes through inhibition of DPP-4. Using field-based QSAR and Schrödinger Maestro suite, the activities of the designed molecules were predicted and compared using docking scores. G86 (pIC50=7.8 nM), G9 (pIC50=8.07 nM), and G82 (pIC50=7.81 nM) showed activity similar to that of the reference molecule A44-Sitagliptin (pIC50=7.74 nM). Molecular docking for ten highly active compounds ranked them based on binding free energy and affinity, revealing that G86 (Glide score = -10.9) had a higher binding affinity than A44-Sitagliptin (Glide score = -9.3). G86 formed hydrogen bonds with TYR 662 and NH_4^+,

TYR 547 and the carbonyl group, and GLU 206 and VAL 207 with the NH_2 group, along with Pi-Pi stacking interactions with PHE 357 and TYR 666, similar to A44, but with more hydrogen-bond interactions. Qikprop predicts the pharmacokinetic and physicochemical (ADME) properties of these molecules. Toxicity prediction for G86 with Pro Tox 3.0 classified it as toxicity class 4 with a predicted LD_{50} of >1000 mg/kg. MD simulations confirmed the stability of G86-1X70, A45-1X70, and A44-Sitagliptin-1X70 complexes, with G86-1X70 showing greater stability than the reference compound. This study suggested that G86 may have higher activity than the existing molecule, warranting further synthesis and in vitro and in vivo studies.

Acknowledgements

The authors are grateful to Schrödinger LLC for providing the trial version of Schrödinger Suite 2022-1 for the field-based QSAR and MD simulation studies.

5. References

1. Kumar S, Mittal A, Mittal A. A review upon medicinal perspective and designing rationale of DPP-4 inhibitors. Bioorganic & Medicinal Chemistry.;46:116354 (2021).

2. Jaiswal S, Gupta P, Prasad LVN, Kulkarni R. An Empirical Model for the Classification of Diabetes and Diabetes_Types Using Ensemble Approaches. Journal of Artificial Intelligence and Technology. 20;3(4):181–6 (2023).

3. Havale SH, Pal M. Medicinal chemistry approaches to the inhibition of dipeptidyl peptidase-4 for the treatment of type 2 diabetes. Bioorganic & Medicinal Chemistry.;17(5):1783–802 (2009).

4. Lei X, Zhou Q, Wang Y, Fu S, Li Z, Chen Q. Serum and supplemental vitamin D levels and insulin resistance in T2DM populations: a meta-analysis and systematic review. Sci Rep.;13(1):12343 (2023).

5. International Diabetes Federation [Internet]. [cited 2024 Jul 31]. Facts & figures. Available from: https://idf.org/about-diabetes/diabetes-facts-figures/

6. Kushwaha RN, Haq W, Katti SB. Discovery of 17 Gliptins in 17-Years of Research for the Treatment of Type 2 Diabetes: A Synthetic Overview.;4 (2014).

7. Bharathi KS, Velmurugan V. Qsar and Docking Studies of New Triazolopiperazine Derivatives as Potent Hypoglycemic Candidates.;6(7):1598–613 (2023).

8. Sawant S, Nerkar A, Pawar ND, Velapure AV. Design, synthesis, QSAR studies and biological evaluation of novel triazolopiperazine based B-amino amides as Dipeptidyl peptidase-iv (DPP-IV) inhibitors: PART-II. International Journal of Pharmacy and Pharmaceutical Sciences.;6:812–7 (2014).

9. Saha B, Das A, Jangid K, Kumar A, Kumar V, Jaitak V. Identification of coumarin derivatives targeting acetylcholinesterase for Alzheimer's disease by field-based 3D-QSAR, pharmacophore model-based virtual screening, molecular docking, MM/GBSA, ADME and MD Simulation study. Current Research in Structural Biology.;7:100124 (2024).

10. Ali A, Abdellattif MH, Ali A, AbuAli O, Shahbaaz M, Ahsan MJ, et al. Computational Approaches for the Design of Novel Anticancer Compounds Based on Pyrazolo[3,4-d]pyrimidine Derivatives as TRAP1 Inhibitor. Molecules.;26(19):5932 (2021).

11. ElMchichi L, Belhassan A, Lakhlifi T, Bouachrine M. 3D-QSAR Study of the Chalcone Derivatives as Anticancer Agents. Journal of Chemistry.;2020(1):5268985 (2020).

12. LigPrep User Manual [Internet]. [cited 2024 Jul 30]. Available from: https://learn.schrodinger.com/private/edu/release/current/Documentation/html/ligprep/ligprep_user_manual/ligprep_user_manualTOC.htm?Highlight=ligprep

13. Kim D, Wang L, Beconi M, Eiermann GJ, Fisher MH, He H, et al. (2 *R*)-4-Oxo-4-[3-(Trifluoromethyl)-5,6-dihydro[1,2,4]triazolo[4,3- *a*]pyrazin- 7(8 *H*)-yl]-1-(2,4,5-trifluorophenyl)butan-2-amine: A Potent, Orally Active Dipeptidyl Peptidase IV Inhibitor for the Treatment of Type 2 Diabetes. J Med Chem.;48(1):141–51 (2005).

14. Bank RPD. RCSB PDB - 1X70: HUMAN DIPEPTIDYL PEPTIDASE IV IN COMPLEX WITH A BETA AMINO ACID INHIBITOR [Internet]. [cited 2024 Jul 30]. Available from: https://www.rcsb.org/structure/1x70

15. Madhavi Sastry G, Adzhigirey M, Day T, Annabhimoju R, Sherman W. Protein and ligand preparation: parameters, protocols, and influence on virtual screening enrichments. J Comput Aided Mol Des.;27(3):221–34 (2013).

16. Saxena S, Abdullah M, Sriram D, Guruprasad L. Discovery of novel inhibitors of *Mycobacterium tuberculosis* MurG: homology modelling, structure based pharmacophore, molecular docking, and molecular dynamics simulations. Journal of Biomolecular Structure and Dynamics.;36(12):3184–98 (2018).

17. Satarker S, Maity S, Mudgal J, Nampoothiri M. In silico screening of neurokinin receptor antagonists as a therapeutic strategy for neuroinflammation in Alzheimer's disease. Mol Divers.;26(1):443–66 (2022).

18. Bouamrane S, Khaldan A, Hajji H, El-mernissi R, Maghat H, Ajana MA, et al. 3D-QSAR, molecular docking, molecular dynamic simulation, and ADMET study of bioactive compounds against candida albicans. Moroccan Journal of Chemistry. 2022 Jun 20;10(3):J. Chem. 523-541 (2022).

19. Friesner RA, Banks JL, Murphy RB, Halgren TA, Klicic JJ, Mainz DT, et al. Glide: A New Approach for Rapid, Accurate Docking and Scoring. 1. Method and Assessment of Docking Accuracy. J Med Chem.;47(7):1739–49 (2004).

20. Jana S, Singh SK. Identification of selective MMP-9 inhibitors through multiple e-pharmacophore, ligand-based pharmacophore, molecular docking, and density functional theory approaches. Journal of Biomolecular Structure and Dynamics.;37(4):944–65 (2019).

21. Patel CN, Jani SP, Jaiswal DG, Kumar SP, Mangukia N, Parmar RM, et al. Identification of antiviral phytochemicals as a potential SARS-CoV-2 main protease (Mpro) inhibitor using docking and molecular dynamics simulations. Sci Rep.;11(1):20295 (2021).